A New Current Limiting and Overload Protection Strategy for Droop-Controlled Voltage-Source Converters in Islanded AC Microgrids Under Grid Faulted Conditions

Zi-lin Li
Department of Electrical Engineering
The Hong Kong Polytechnic University
Hong Kong, Hong Kong SAR
zi-lin.li@connect.polyu.hk

Jiefeng Hu
School of Engineering, Information Technology and Physical Sciences
Federation University Australia
Mount Helen, Australia
j.hu@federation.edu.au

Ka Wing Chan
Department of Electrical Engineering
The Hong Kong Polytechnic University
Hong Kong, Hong Kong SAR
eekwchan@polyu.edu.hk

***Abstract*—Grid-forming voltage source converter (VSC) plays a vital role in the future renewable energy-based utility grid. Limited by the thermal capability of semiconductor switches, grid-forming VSC-based distributed generation units (DGs) cannot stand excess overcurrent like synchronous generators (SG) during large transient disturbances. In order to protect the VSC from overcurrent and ride through the transient disturbances, a new current limiting and overload protection strategy is proposed in this paper. By properly selecting the maximum current thresholds in the synchronous rotating frame, overcurrent and overload protection are achieved simultaneously. The synchronization among DGs is enhanced by feeding back the output voltage in the q-axis to the active power droop control. A comparison study between the proposed strategy and two existing methods are conducted using a networked microgrid in PSCAD/EMTDC, examining the effectiveness of the proposed strategy.**

Keywords—grid-forming converter, current limiting, transient disturbances, fault ride-through capability, microgrid

I. INTRODUCTION

Due to the inherent characteristics of renewable energy sources (RES), a power electronic converter is required to transfer renewable power to the utility grid. For most of the power converters belonging to RES-based distributed generation units (DGs), they are controlled as grid-follower to inject powers according to the maximum power point (MPP) or power references from their upstream hierarchical controllers [1]. The grid-following converters can track their power references accurately; however, they fail to operate in island mode. Stability issues also arise under weak grid conditions.

For energy transition from the synchronous generator (SG)-based electrical system to a RES-based one, grid-forming voltage-source converters (VSC) are now attracting more and more attention from researchers [2]. Instead of following the utility grid, grid-forming VSCs are controllable voltage sources and can establish their voltage amplitude and frequency at the point of connection. Thus, a grid-forming converter is able to work at both the grid-connected and islanded modes. Several control strategies have been proposed in existing literature to realize functions of the grid-forming VSC, including droop control, synchronverter, virtual synchronous machine, and synchronous power control, etc. [3, 4]. Though a grid-forming VSC can mimic the steady-state characteristics of a SG, it lacks spinning energy reserve and is more sensitive to transient events, such as large load connection or grid faults. Besides, similar to SGs, the grid-forming VSC can also experience transient instability under large disturbance conditions.

During grid short-circuit faults, a SG can typically withstand a large output current up to 6-8 pu [3]. However, the thermal limit of semiconductor switches allows the converter to supply an overcurrent only about 1.2-1.4 pu [5]. A common method to protect the converter from any overcurrent damages is to trip it from the system whenever a grid fault is detected. Yet, for a future RES-based utility system, the grid-forming VSCs should have the ability to ride through grid faults / large disturbances and undertake the responsibility to support the grid voltage and frequency. The low-voltage ride-through (LVRT) function has been widely adopted in wind power systems and extended to PV systems with the grid-following converters [6]. Some strategies can also be found in the existing literature to improve the performance of a grid-forming VSC when suffering from large transient disturbances.

For overcurrent protection of a grid-forming VSC, several strategies found in literature can be categorized into 1) additional hardware-based method [7-9], 2) virtual impedance-based strategy [10-12], 3) current limiting droop control [13, 14], 4) switching control mode strategy [3, 15], 5) software limiter-based approach [16, 17], and 6) enhanced semiconductor switch[18].

In the additional hardware-based method, series voltage-source inverter (VSI) [7], superconductive fault current limiter (SFCL) [8], unidirectional fault current limiter [9], etc. are used to limit the output current of a grid-forming VSC or the current flowing between a microgrid and its upstream grid. The current limiting of the enhanced semiconductor switch in [18] is achieved by changing its physical characteristics with the integration of a phase-change material. These two types of methods realize overcurrent protection via hardware manipulation. However, the methods will not only increase the total cost and system complexity but also reduce system reliability. They may not be appropriate for grid-forming VSC-based DGs as the number of DGs keeps increasing significantly in the distribution network.

The other four types of methods mainly modify the control strategies of a grid-forming VSC in software, which are cost-free and able to equip the VSC with more intelligence. The basic idea of the virtual impedance-based method [10-12] is to reduce voltage references for the grid-forming VSCs when the output current exceeds a predefined threshold, without any control mode switching or fault

detection. Nevertheless, the effectiveness of this method highly depends on factors like fault locations, network impedance, and the selected virtual impedance. A large virtual impedance value could introduce instability issues. Instead of utilizing the previously mentioned grid-forming control strategies, the current limiting is designed inherently in a new droop controller [13, 14]. The nonlinear input-to-state theory is used to analyze the performance; however, it is not easy to select proper parameters for the controller. The switching control method [3, 15] is also a popular strategy to limit the output current. As soon as a grid fault is detected, the grid-forming VSC is switched from the voltage-controlled mode to a current-controlled mode, outputting constant currents or powers. Though the current limiting and fault ride-through capability can be obtained during grid faults, the converter loses the output voltage controllability. This may not be desirable when considering the high penetration of DGs, complicate network impedance and various grid faults. The accuracy of fault detection and clearance highly determines the performance of this method. Simple software instantaneous limiter is also a common strategy for current limiting, which can be used in the synchronous reference frame (SYRF), stationary reference frame (STRF), and natural reference frame (NARF) [16]. To improve the transient stability, stability enhanced *P-f* droop control [17] is implemented together with the instantaneous limiter. An anti-windup strategy is usually necessary for the voltage and current controllers of a VSC; however, the transient performance would depend on the anti-windup feedback gain and grid fault levels.

Though the above mentioned strategies can improve the performance of a grid-forming VSC during grid faults, proper overcurrent protection is still challenging with the consideration of grid fault types, transient stability, and synchronization issues. Different from SGs, grid-forming VSCs powered by RES usually have limited active power.

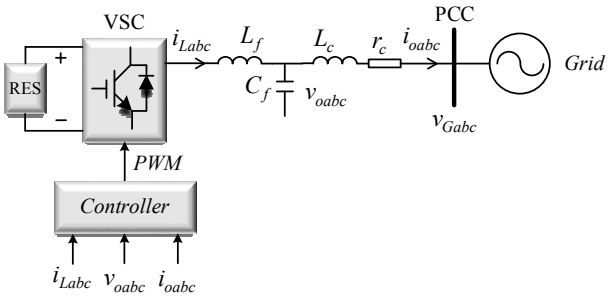

Fig. 1. A droop-controlled VSC-based DG connected to a power grid.

Therefore, the current limiting strategy should also ensure the active power output not exceeding the allowed limit, which however has been rarely considered. In this paper, a new current limiting and overload protection strategy is presented. The proposed strategy is based on instantaneous limiters in the SYRF. The voltage term in the *q*-axis contains information of the power angle, and is fed back to the *P-f* droop controller for synchronization enhancement. A comparison simulation study between the proposed and two existing strategies is presented to examine the effectiveness of the proposed strategy.

II. THE PROPOSED CURRENT LIMITING AND OVERLOAD PROTECTION STRATEGY

As shown in Fig. 1, a droop-controlled VSC-based DG is connected to an infinite AC grid for developing the proposed strategy. The energy from RES is injected into the grid via a three-phase two-level voltage source converter. An LC filter with inductance L_f and capacitance C_f is necessary to attenuate the switching ripples. A line with L_c and r_c connects the DG to an infinite ac bus. The conventional *P-f* and *Q-V* droop control strategy is adopted to realize the grid-forming characteristics of the DG, as shown in Fig. 2. To obtain the averaged power signals, a

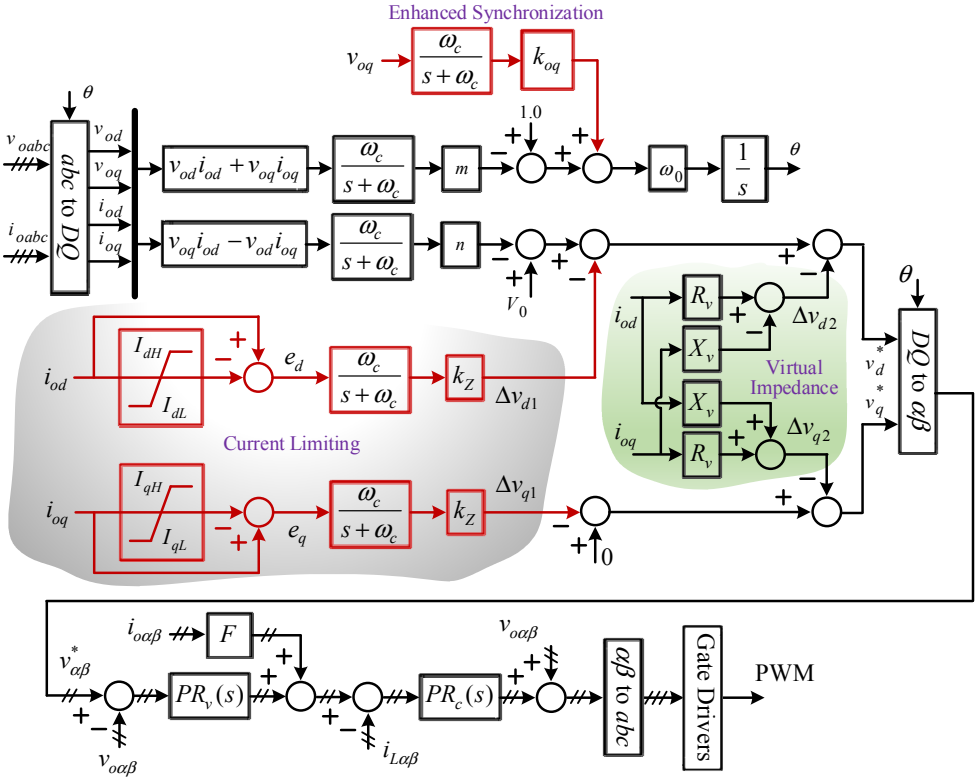

Fig. 2. Controller diagram of a droop-controlled VSC-based DG with the proposed current limiting strategy.

low-pass filter (LPF) with cutoff frequency ω_c is inserted into the droop controller. Droop coefficients m and n are per-unit values and dependent on the maximum allowed voltage and frequency deviations. The setting voltage amplitude of the reactive droop control is V_0. A virtual impedance loop with R_v/X_v=1 is utilized to reduce couplings between the active and reactive power droops. After the voltage references are generated by the droop controller, they are transformed into the stationary frame and fed to the inner voltage and current control loop with proportional and resonant (PR) controllers.

A. The proposed strategy and selection of the thresholds

A droop-controlled VSC is to regulate the amplitude and frequency of the output voltage for achieving a proper power-sharing with other sources, its output current is sensitive to variations of the grid voltage. Besides, the close electrical proximity of DGs to each other in a low-voltage distribution network can degrade the system transient performance as well.

When the voltage at the point of common coupling (PCC) experiences a sag caused by a large load connection or a grid fault, the large voltage drops on the connecting line will drive the DG output current up. Then an overcurrent scenario would occur, which should be avoided for the VSC protection. Meanwhile, grid-supporting capability requires the VSC to output current as large as possible. In order to achieve current limiting and grid supporting simultaneously, a new strategy is proposed as shown in Fig. 2. The strategy is implemented in the SYRF, differences between the actual output currents and the predefined values are defined as

$$e_d = \begin{cases} i_{od} - I_{dH}, & i_{od} > I_{dH} \\ 0, & I_{dL} \le i_{od} \le I_{dH} \\ i_{od} - I_{dL}, & i_{od} < I_{dL} \end{cases}$$
$$e_q = \begin{cases} i_{oq} - I_{qH}, & i_{oq} > I_{qH} \\ 0, & I_{qL} \le i_{oq} \le I_{qH} \\ i_{oq} - I_{qL}, & i_{oq} < I_{qL} \end{cases} \quad (1)$$

where I_{dH} and I_{dL} are the upper and lower limit of the d-axis current, while I_{qH} and I_{qL} are the defined limits of the q-axis current. When the output currents in the SYRF are within the defined range, the current errors will be zero and the DG is operating normally. Whenever the current error is non-zero, it means that the corresponding current component is larger than the threshold, and an additional voltage term will be generated by the current error and subtracted from the droop voltage references. The proposed strategy works like a proportional controller to regulate the current errors close to zero. As a result, the DG can contribute its maximum value to the grid fault current.

Different from the conventional SGs, a VSC-based DG can work in four-quadrants to inject or absorb active and reactive powers. Besides, a DG powered by RES usually has a limited active power capacity. So, the output active power should be limited within the allowed range even during large transient disturbances. Under normal steady-state conditions, the output active and reactive power can be calculated as functions of the output current as follows.

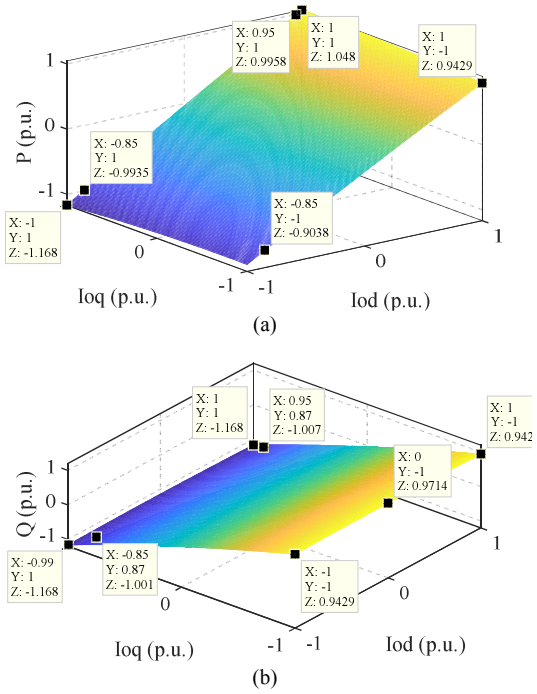

Fig. 3. When I_{od} and I_{oq} vary within range [-1.0, 1.0] pu, the possible power values: (a) active power, (b) reactive power.

$$\begin{cases} P = \dfrac{I_{od}}{1 - nI_{oq}}\left[V_0 + X_v\left(I_{oq} + nI_{od}^2\right)\right] - R_v\left(I_{od}^2 + I_{oq}^2\right) - X_v I_{od} I_{oq} \\ Q = \dfrac{-I_{oq}}{1 - nI_{oq}}\left[V_0 + X_v\left(I_{oq} + nI_{od}^2\right)\right] - X_v I_{od}^2 \end{cases} \quad (2)$$

where I_{od} and I_{oq} are the d- and q-axis components of the output current under steady-state conditions. With V_0 = 1.05 pu, n = 0.05 pu, and the virtual impedance R_v = X_v = 0.03 pu, the output powers are plotted when the output current varies, as shown in Fig. 3.

In Fig.3, the active and reactive powers vary with the output currents. When P and Q are positive values, it means that the DG is injecting powers into the grid, and vice versa. As shown in Fig. 3, though the output current components are within the rated range, P and Q can exceed the rated values. To provide current limiting and overload protection at the same time in this paper, the upper and lower limits of d- and q-axis current are selected as

$$\begin{cases} I_{dH} = 0.95\,p.u. \\ I_{dL} = -0.85\,p.u. \end{cases}, \begin{cases} I_{qH} = 0.87\,p.u. \\ I_{qL} = -1.0\,p.u. \end{cases} \quad (3)$$

B. Enhanced synchronization

In the droop controller, the reference voltage of the q-axis is usually set to zero. Under normal operation, the output voltage is aligned with the d-axis and the inserted virtual impedance does not affect the alignment much. However, due to the proposed current limiting strategy, v_{oq} of a DG may deviate from zero significantly during grid faults, leading to a large phase difference between the DG and the rest of the grid. Therefore, to improve transient performance, an enhanced synchronization is added to the P-f droop control [17], as shown in Fig. 2. The enhanced synchronization control is similar to a phase-locked loop (PLL), regulating v_{oq} close to zero by altering the droop frequency.

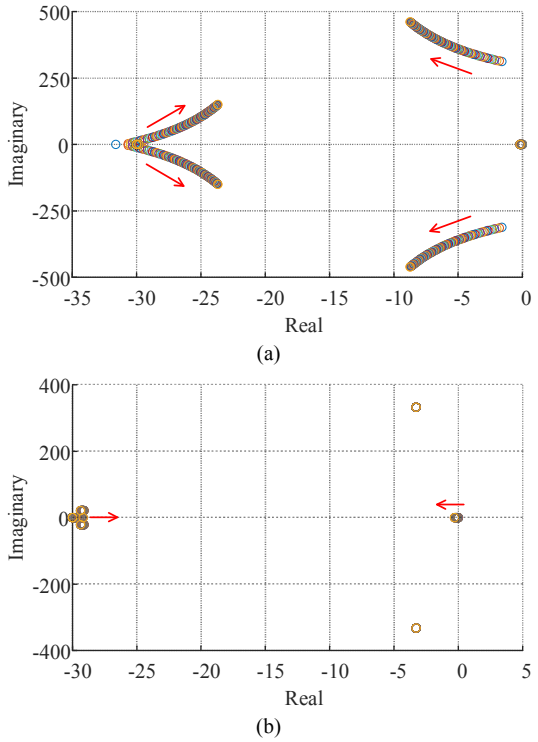

Fig. 4. The root-locus of the system when (a) k_{oq}=0.2, k_Z varies from 0 to 100; (b) k_Z=10, k_{oq} varies from 0 to 1.

C. Small-signal stability analysis

With the proposed strategy, a grid-forming VSC-based DG will present different characteristics during large transient disturbances. Two parameters k_Z and k_{oq} should be designed properly to realize the current limiting and ensure a stable operation. Therefore, a small-signal model of the system in Fig. 1 is developed to investigate the stability issues and select proper values for k_Z and k_{oq}. The inner voltage and current controllers are neglected due to their negligible influence on low-frequency stability. With consideration of the droop controller, the proposed strategy, and the connecting line, a small-signal model with eight state variables is built in the SYRF,

$$\begin{bmatrix}\dot{X}_{DG}\\ \dot{X}_c\end{bmatrix}=\begin{bmatrix}A_{DG} & B_{DG1}\\ B_cC_{DG}-B_cE & A_c+B_cD_{DG}\end{bmatrix}\begin{bmatrix}X_{DG}\\ X_c\end{bmatrix}-\begin{bmatrix}0_{6\times2}\\ B_cT\end{bmatrix}\hat{v}_{bDQ}-\begin{bmatrix}1\\ 0_{7\times1}\end{bmatrix}\Delta\omega_{com} \quad (4)$$

where $\dot{X}_{DG}, \dot{X}_c$ are the state variables of the DG and the connecting line, respectively. $\hat{v}_{bDQ}$ is the PCC voltage vector under the reference frame. The details of the other components are listed in the Appendix. When there is a grid fault, the DG would usually output the maximum active and reactive power driving the I_{od} to the upper limit and the I_{oq} to the lower limit, i.e. I_{od}=0.95pu, I_{oq}=−1.0pu. The DG in Fig. 1 has a rated power S_N=10kVA and its parameters are listed in Table I. The inductance and resistance of the connecting line are L_c=0.043pu and r_c=0.041pu, respectively, taking the rated power of the DG as the base value. Selecting the output current I_{od}=0.95pu and I_{oq}=−1.0pu for the operating point, the root locus of the system is plotted in Fig. 4 with varying k_Z and k_{oq}.

As shown in Fig. 4(a), as k_Z varies from 0 to 100, the eigenvalues of the system are always on the left-hand side plane, indicating a stable system. However, a large k_Z will increase the imaginary part of the dominant roots, causing a more oscillatory system. While the root-locus in Fig. 4(b) shows that k_{oq} has little influence on system stability, a small value of k_{oq} should be selected to limit its influence on the active power-sharing accuracy.

TABLE I. PARAMETERS OF DGS IN SIMULATION

Symbol	*Description*	*Values*
V_N	Rated peak value	311V
f_0	Rated system frequency	50Hz
S_{N1}/S_{N2}	Rated power of DG1/DG2	10/20kVA
S_{N3}/S_{N4}	Rated power of DG3/DG4	50/30kVA
f_s	Switching frequency	20*k*Hz
V_{dc}	DC voltage	800*V*
V_0	Setting votlage point	1.05p.u.
L_f	Filter inductance	0.059p.u.
C_f	Filter capacitance	0.2p.u.
L_c	Output line impedance of DGs	0.018p.u.
R_v , X_v	Virtual resistance and reactance	0.03p.u.
PR_v	PR voltage controller	k_{pv}=1.2, k_{iv}=1000
k_{pc}	Current controller	8
F	Feedforward gain	0.6
m	Active power droop gain	0.01p.u.
n	Reactive power droop gain	0.05p.u.
ω_c	Cutoff frequency of LPF	30rad/s
k_Z	Gain of current limitng strategy	25
k_{oq}	Enhanced synchronization gain	0.15
I_{max}	Maximum current magnitude	1.414p.u.

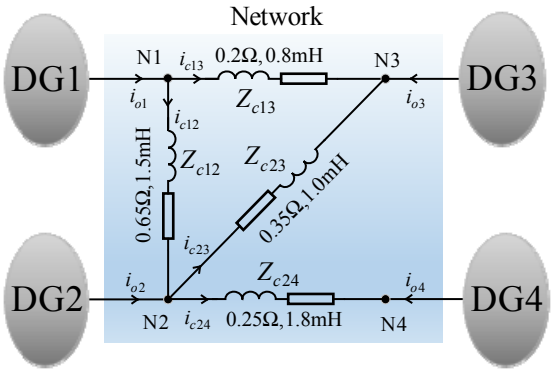

Fig. 5 An islanded microgrids with four droop-controlled DGs.

III. SIMULATION RESULTS AND COMPARISON STUDY

To verify the effectiveness of the proposed current limiting strategy in a grid-forming VSC-based system, an islanded microgrid as shown in Fig. 5 is built in PSCAD/EMTDC. Parameters of the DGs have listed in Table I. The virtual impedance-based strategy in [11] and the limiter-based stability enhanced P-f droop control (SEPFC) in [17] are also implemented for comparison study. In the virtual impedance-based strategy, the proportional gain $k_{p,Rvi}$ = 0.2, impedance ratio X/R = 3, and current threshold is 1.0pu. The proportional gain is k_{oq} =0.15 in the SEPFC and the maximum current magnitude is 1.414pu.

In the beginning, there is a resistive load R=10Ω connected to node N2. At t=1.0s, a three-phase fault occurs at N3 with Z_f=0.2Ω, and it is cleared 2 seconds later.

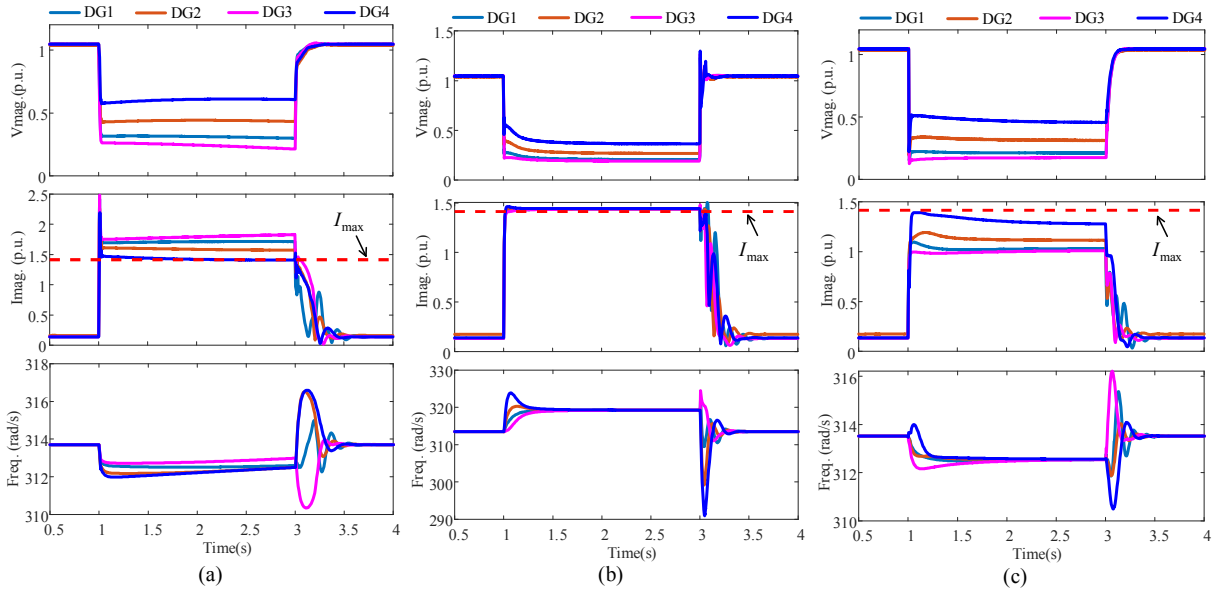

Fig. 6 Simulation results for the output voltage magnitude, output current magnitude, and frequency of the DGs with different current limiting strategies: (a) virtual impedance-based method in [11]; (b) stability enhanced P-f droop control in [17]; and (c) the proposed method.

The performance of DGs using the virtual impedance method is shown in Fig. 6(a) when the fault is applied and cleared. As illustrated from the simulation results in Fig. 6(a), during the grid faults, the output voltages of all DGs are reduced significantly and the current magnitudes are limited owing to the current limiting virtual impedance. However, the output currents of DG1, DG2, and DG3 are higher than the maximum value, among which the DG3 has the highest value, about 30% higher than the maximum limit due to its proximity to the fault. While the DG4 current can be limited within the range. This illustrates that the current limiting performance depends on the equivalent impedance between the fault point and the DGs. Besides, the waveforms of the DGs' frequencies in Fig. 6(a) shows that they cannot reach a common value during the fault, indicating that the output voltages and currents are not able to settle on a steady-state point. This is not desirable, especially when the fault cannot be cleared timely.

The SEPFC method can be easily implemented in the DGs to achieve current limiting and enhanced transient stability performance during grid faults, as shown in Fig. 6(b). Different from the virtual impedance method, the SEPFC method can accurately limit the output current magnitude of all DGs to the maximum value, and the frequencies also converge to a common value quickly. Though the currents are at the maximum value, the output voltage magnitudes of the DGs are relatively lower than that with the virtual impedance method and the proposed method, meaning that the SEPFC method has a weak voltage supporting capability during the fault. After the fault is cleared, some DGs experience a transient overvoltage and a very large fluctuation of frequency.

When the DGs are equipped with the proposed strategy, the system performance is illustrated in Fig. 6(c). As one can find that the output current magnitudes of all DGs are limited effectively within the maximum value during the fault, and the frequencies converge to an identical value in about 1.5s. Fig. 7 shows performance in detail as the output current is limited in the *d*- and *q*-axis separately. When the grid fault occurs, the DGs inevitably experience a transient

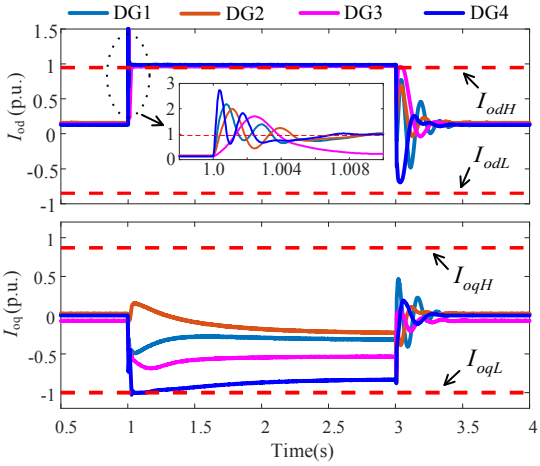

Fig. 7 Simulation results of the d- and q-aixs output current components of the DGs using the proposed current limiting strategy.

overshoot on the *d*-axis current due to the limited bandwidth of the inner controllers. The maximum current could reach as high as 2.8pu. After about 5ms the inner controllers become active and the currents in the *d*- and *q*-axis are limited by the proposed strategy within the predefined range. The actual currents in the *d*-axis shown in Fig. 7 are about 0.03pu higher than the predefined upper limit. This error is necessary to generate additional voltage terms for achieving the current limiting. A higher value of k_Z can slightly reduce the error. The voltage magnitudes of the DGs in Fig. 6(c) are slightly lower than that with the virtual impedance method, yet, higher than that with the SEPFC. In the recovery, the output voltages rise smoothly without an over-voltage phenomenon. The frequency fluctuation is also much smaller than that using SEPFC.

IV. CONCLUSION

With the increasingly high penetration of grid-forming VSC-based DGs in the utility grid, it becomes more important to protect the DGs from overcurrent and overload during large transient disturbances. In this paper, a new current limiting and overload protection is proposed for

droop-controlled VSC-based DGs. It is easy to realize in the DG controller and can limit active and reactive power separately. With proper selection of the current threshold, overcurrent and overload protection can be achieved simultaneously. Comparing with the virtual impedance-based and SEPFC methods in the simulation, the proposed strategy appears to have accurate current limitations and good voltage supporting performance during a resistive three-phase bolted fault.

REFERENCE

[1] J. Rocabert, A. Luna, F. Blaabjerg, and P. Rodriguez, "Control of power converters in ac microgrids," IEEE Trans. Power Electron., vol. 27, no. 11, pp. 4734-4749, Nov 2012.

[2] R. H. Lasseter, Z. Chen, and D. Pattabiraman, "Grid-forming inverters: A critical asset for the power grid," IEEE Trans. Emerg. Sel. Topics Power Electron., vol. 8, no. 2, pp. 925-935, 2020.

[3] M. G. Taul, X. Wang, P. Davari, and F. Blaabjerg, "Current limiting control with enhanced dynamics of grid-forming converters during fault conditions," IEEE Trans. Emerg. Sel. Topics Power Electron., pp. 1-1, 2019.

[4] J. Hu, J. Zhu, and J. M. Guerrero, "Model predictive control of smart microgrids," in 2014 17th International Conference on Electrical Machines and Systems (ICEMS), 2014: IEEE, pp. 2815-2820,

[5] S. F. Zarei, H. Mokhtari, M. A. Ghasemi, and F. Blaabjerg, "Reinforcing fault ride through capability of grid forming voltage source converters using an enhanced voltage control scheme," IEEE Trans. Power Delivery, vol. 34, no. 5, pp. 1827-1842, 2019.

[6] J. Hu, Z. Li, J. Zhu, and J. M. Guerrero, "Voltage stabilization: A critical step toward high photovoltaic penetration," IEEE Ind. Electron. Mag., vol. 13, no. 2, pp. 17-30, 2019.

[7] D. M. Vilathgamuwa, P. C. Loh, and Y. Li, "Protection of microgrids during utility voltage sags," IEEE Trans. Ind. Electron., vol. 53, no. 5, pp. 1427-1436, 2006.

[8] D. M. Yehia and D.-E. A. Mansour, "Modeling and analysis of superconducting fault current limiter for system integration of battery banks," IEEE Trans. Appl. Supercond., vol. 28, no. 4, pp. 1-6, 2018.

[9] T. Ghanbari and E. Farjah, "Unidirectional fault current limiter: An efficient interface between the microgrid and main network," IEEE Trans. Power Syst., vol. 28, no. 2, pp. 1591-1598, 2012.

[10] F. Salha, F. Colas, and X. Guillaud, "Virtual resistance principle for the overcurrent protection of pwm voltage source inverter," in 2010 IEEE PES Innovative Smart Grid Technologies Conference Europe (ISGT Europe), 2010: IEEE, pp. 1-6,

[11] A. D. Paquette and D. M. Divan, "Virtual impedance current limiting for inverters in microgrids with synchronous generators," IEEE Trans. Ind. Appl., vol. 51, no. 2, pp. 1630-1638, 2014.

[12] X. Lu, J. Wang, J. M. Guerrero, and D. Zhao, "Virtual-impedance-based fault current limiters for inverter dominated ac microgrids," IEEE Trans. Smart Grid, vol. 9, no. 3, pp. 1599-1612, 2016.

[13] Q.-C. Zhong and G. C. Konstantopoulos, "Current-limiting droop control of grid-connected inverters," IEEE Trans. Ind. Electron., vol. 64, no. 7, pp. 5963-5973, 2017.

[14] A. G. Paspatis and G. C. Konstantopoulos, "Three-phase current-limiting droop controlled inverters operating in parallel," in 2019 IEEE Milan PowerTech, 2019: IEEE, pp. 1-6,

[15] K. Shi, W. Song, P. Xu, R. Liu, Z. Fang, and Y. Ji, "Low-voltage ride-through control strategy for a virtual synchronous generator based on smooth switching," IEEE Access, vol. 6, pp. 2703-2711, 2018.

[16] I. Sadeghkhani, M. E. H. Golshan, J. M. Guerrero, and A. Mehrizi-Sani, "A current limiting strategy to improve fault ride-through of inverter interfaced autonomous microgrids," (in English), IEEE Trans. Smart Grid, vol. 8, no. 5, pp. 2138-2148, Sep 2017.

[17] L. Huang, H. Xin, Z. Wang, L. Zhang, K. Wu, and J. Hu, "Transient stability analysis and control design of droop-controlled voltage source converters considering current limitation," IEEE Trans. Smart Grid, vol. 10, no. 1, pp. 578-591, 2019.

[18] W. Shao et al., "A power module for grid inverter with in-built short-circuit fault current capability," IEEE Trans. Power Electron., pp. 1-1, 2020.

APPENDIX

The state variables of the DG

$$X_{DG} = \begin{bmatrix} \Delta\delta & \Delta P & \Delta Q & \Delta y_{oq} & \Delta v_{d1} & \Delta v_{q1} \end{bmatrix}^T,$$

Here

$$\Delta y_{oq} = \frac{\omega_c}{s+\omega_c}\Delta v_{oq}$$

The state variables of the connecting line:

$$X_c = \begin{bmatrix} \Delta i_{od} & \Delta i_{oq} \end{bmatrix}^T.$$

The matrixes of the system:

$$A_{DG} = \begin{bmatrix} 0 & -m & 0 & k_{oq} & 0 & 0 \\ 0 & -\omega_c & -n\omega_c I_{od} & 0 & -\omega_c I_{od} & -\omega_c I_{oq} \\ 0 & 0 & -\omega_c + n\omega_c I_{oq} & 0 & \omega_c I_{oq} & -\omega_c I_{od} \\ 0 & 0 & 0 & -\omega_c & 0 & -\omega_c \\ 0 & 0 & 0 & 0 & -\omega_c & 0 \\ 0 & 0 & 0 & 0 & 0 & -\omega_c \end{bmatrix}$$

$$B_{DG} = \begin{bmatrix} 0 & 0 \\ \omega_c\left(V_{od} - R_v I_{od} - X_v I_{oq}\right) & \omega_c\left(V_{oq} - R_v I_{oq} + X_v I_{od}\right) \\ \omega_c\left(V_{oq} + R_v I_{oq} - X_v I_{od}\right) & -\omega_c\left(V_{od} - R_v I_{od} - X_v I_{oq}\right) \\ -\omega_c X_v & -\omega_c R_v \\ k_Z\omega_c & 0 \\ 0 & k_Z\omega_c \end{bmatrix}$$

$$C_{DG} = \begin{bmatrix} 0 & 0 & -n & 0 & -1 & 0 \\ 0 & 0 & 0 & 0 & 0 & -1 \end{bmatrix}, D_{DG} = \begin{bmatrix} -R_v & X_v \\ -X_v & -R_v \end{bmatrix}$$

$$A_c = \begin{bmatrix} -\frac{r_c}{L_c} & \omega_{com} \\ -\omega_{com} & -\frac{r_c}{L_c} \end{bmatrix}, B_c = \begin{bmatrix} \frac{1}{L_c} & 0 \\ 0 & \frac{1}{L_c} \end{bmatrix}, T = \begin{bmatrix} \cos\delta_0 & \sin\delta_0 \\ -\sin\delta_0 & \cos\delta_0 \end{bmatrix}$$

$$E = \begin{bmatrix} -V_{bD}\sin\delta_0 + V_{bQ}\cos\delta_0 & 0 & 0 & 0 & 0 & 0 \\ -V_{bD}\cos\delta_0 - V_{bQ}\sin\delta_0 & 0 & 0 & 0 & 0 & 0 \end{bmatrix}$$